Author/s:
Syed, N;Nguyen, CK;Zavabeti, A;Low, MX;Wei, X;Krishnamurthi, V;Irfan, M;Lee, WSL;Duong, NMH;Nguyen, AT;Reineck, P;Bao, L;Roberts, A;Daeneke, T

Title:
Vacuum-Free Liquid-Metal-Printed 2D Semiconducting Tin Dioxide: The Effect of Annealing

Date:
2024

Citation:
Syed, N., Nguyen, C. K., Zavabeti, A., Low, M. X., Wei, X., Krishnamurthi, V., Irfan, M., Lee, W. S. L., Duong, N. M. H., Nguyen, A. T., Reineck, P., Bao, L., Roberts, A. & Daeneke, T. (2024). Vacuum-Free Liquid-Metal-Printed 2D Semiconducting Tin Dioxide: The Effect of Annealing. ACS Applied Electronic Materials, 6 (12), https://doi.org/10.1021/acsaelm.3c01842.

Persistent Link:
https://hdl.handle.net/11343/345035

Vacuum-Free Liquid-Metal-Printed 2D Semiconducting Tin Dioxide: The Effect of Annealing

Nitu Syed[1,2§], Chung Kim Nguyen[2§]*, Ali Zavabeti[2,3], Mei Xian Low[2], Xiaotian Wei[2], Vaishnavi Krishnamurthi[2], Mehmood Irfan[2], Wendy S.L. Lee[4], Ngoc M. H. Duong[5], Anh Thai Nguyen[6,7], Philipp Reineck[8], Lei Bao[2], Ann Roberts[1], Torben Daeneke[2]*

[1] School of Physics, ARC Centre of Excellence for Transformative Meta-Optical Systems, The University of Melbourne, VIC 3010, Australia

[2]School of Engineering, RMIT University, Melbourne, VIC 3001, Australia

[3]Department of Chemical Engineering, The University of Melbourne, Parkville, VIC 3010, Australia

[4] School of Electrical Engineering and Telecommunications, The University of New South Wales, Sydney, NSW 2033, Australia

[5]CSIRO Manufacturing, West Lindfield, NSW 2070, Australia

[6]Department of Chemical Engineering, Ho Chi Minh City University of Technology (HCMUT), 268 Ly Thuong Kiet Street, District 10, Ho Chi Minh City, Vietnam

[7]Vietnam National University Ho Chi Minh City, Linh Trung Ward, Thu Duc City, Ho Chi Minh City, Vietnam

[8]ARC Centre of Excellence for Nanoscale BioPhotonics, School of Science, RMIT University, Melbourne, VIC 3001, Australia

*E-mail: nitu.syed@unimelb.edu.au, chung.nguyen2@rmit.edu.au

Keywords: Liquid metal, tin oxide, semiconductors, thin film transistors, thermal annealing

Abstract

Ultra-thin film transistors (TFTs) offer unparalleled opportunities for the fabrication of multifunctional electronic and optoelectronic devices. In this work, we report a vacuum-free liquid metal exfoliation technique for rapidly printing ~2-nm-thick layer of oxide from molten tin. We explore the effect of rapid thermal annealing at 450 °C on the stoichiometry, morphology, and

crystal structure of the resulting tin oxide nanosheets. The annealed samples exhibit a dominant SnO_2 phase and a high degree of transparency (>99 %) in the visible spectra. Field-effect transistors based on the two-dimensional (2D) SnO_2 films show typical *n*-channel conduction with a field-effect mobility of ~7.5 $cm^2\ V^{-1}\ s^{-1}$. Photodetectors utilizing annealed tin dioxide demonstrate significant improvement in photoresponsivity reaching a value of 5.2×10^3 $A\ W^{-1}$ compared to that found in an unannealed sample at an ultraviolet wavelength of 285 nm. We demonstrate that the improvement in device performance is due to nanocrystalline changes within the oxide layers during the annealing process. This work offers a straightforward and ambient air-compatible method for depositing ultra-thin, large-area semiconducting oxides as potential candidates for enabling emerging applications in transparent nanoelectronics and optoelectronics.

Introduction

Transparent semiconducting metal oxides (MOXs), particularly those of post-transition metals, are emerging as a promising and technologically important family of two-dimensional (2D) materials with unique optical and electronic characteristics, excellent air stability, and rich surface chemistry.[1-4] These materials have attracted significant attention in a wide range of applications, including electronics/optoelectronics, sensing, catalysis, electrochemistry, and energy storage.[4-8] Although various approaches have been established for realizing 2D MOXs, most conventional synthesis routes rely on either low-yield exfoliation methods or complex vacuum-based deposition techniques.[3, 5] This underscores the high demand for a more straightforward, scalable, and cost-effective synthesis of 2D MOXs.

Liquid metal (LM) printing techniques, introduced in 2017, highlight a new platform for producing high-quality 2D MOXs.[9] Relying on the self-limiting oxidation process of LMs (well described by the Cabrera–Mott oxidation model), this technique enables the direct transfer of surface oxide skin onto relevant substrates.[9-11] With current progress in liquid metal printing methods, several stratified and unstratified MOXs have been produced over large areas with minimal imperfections,[12-14] signifying the compatibility of this synthesis approach with existing industrial manufacturing processes.[15-18]

Among various liquid metal-derived MOXs, tin oxide (SnO_x) is of particular interest in its 2D morphology due to its excellent optical transparency, adjustable electronic properties, and

promising surface chemistry.[19-21] Hence, the atomically thin tin oxide can be utilized in the design of 2D chem-FETs and gas sensors, as well as in the application of catalysis.[5, 20] Furthermore, the reduction in thickness to only a few nanometers considerably increases the mechanical pliability of the nanosheets, highlighting their capability to underpin the development of new types of 2D flexible and wearable nanoelectronics.[22] These tin oxide films can exhibit either *p*- or *n*-type semiconducting characteristics, depending on whether a particular film is in the form of tin (II) oxide (SnO) or tin (IV) oxide (SnO_2), respectively.[19] Large area, atomically thin SnO_x has been harvested from the surface of molten tin,[20] stimulating wide-range of studies into LM-derived 2D SnO_x and its applications over the past few years (Supporting Table S1).[21, 23-27] It is well-established that LM printing in an oxygen-deficient environment (e.g., a glove box) leads to the formation of *p*-type 2D tin monoxide (SnO) nanosheets.[20] When the synthesis was conducted in ambient air, however different stoichiometries of tin oxide were reported, including SnO,[26] SnO_2,[24] and mixed-phase SnO_x[19, 21], leading to considerable inconsistencies in the literature It is worth noting here that SnO is not only different from SnO_2 in terms of its stoichiometry and semiconducting properties but also features a distinctly different crystal structure. SnO exhibits a tetragonal litharge layered structure,[28] whereas its more oxidized counterpart (i.e., SnO_2) forms an unstratified lattice.[19, 20] Moreover, the precise nature of these oxide phases remains poorly understood. Further research is necessary to address the crystal structure that arises due to temperature variations during synthesis. Hence, a comprehensive investigation into the chemical composition and crystalline structure of air-synthesized 2D SnO_x is crucial for gaining insights into LM chemistry and understanding the electronic properties of this technologically promising material.

In this work, we prepare 2D SnO_x nanosheets in ambient conditions by using an instant in air LM touch-printing technique. The effects of air-aging and thermal-annealing on the morphology and chemical composition of the obtained nanosheets are investigated. Transmission electron microscopy and atomic force microscopy are employed to observe changes within the oxide nanosheets before and after the annealing process. We demonstrate that implementing a rapid post-synthesis annealing process of 15 minutes at 450 °C results in a significant reduction in the crystal disorder with a dominant phase of SnO_2. Consequently, an enhancement of two-orders of magnitude is realized in the mobility of field effect transistors (FETs) fabricated using these SnO_2 nanosheets as well as a significant improvement in solar-blind UV detector performance.

Discussion

The synthesis of 2D tin oxide nanosheets was performed in an ambient atmosphere by leveraging a vacuum-free liquid metal-based van der Waal (vdW) transfer technique (see Experimental section and Figure 1a).[9, 13, 20, 22] 2D SnO_x naturally grows on the surface of molten tin in the presence of oxygen.[19, 20] The weak adhesion between the oxide skin and the parent liquid metal enables the direct transfer of 2D oxide nanosheets onto suitable substrates.[9, 13] The ultrathin nanosheets obtained from the freshly preconditioned molten tin have minimal variability in thickness across a large lateral area of several mm^2 (Figure 1b and Supporting Figure S1b).

It has been previously reported that the 2D SnO_x printed from molten tin under atmospheric conditions consists of both tin mono oxide (SnO) and tin dioxide (SnO_2).[19, 20] Indeed, our X-ray photoelectron spectroscopy (XPS) data of as-deposited 2D nanosheets indicate a remarkable amount of SnO which was gradually oxidized into a SnO_2 stoichiometry when aging in ambient conditions. However, the presence of SnO is still evident after 4 weeks of air exposure (Supporting Figure S2a). This can also be observed from the valence band photoemission spectra (VB-XPS) analysis (Supporting Figure S2b). VB-XPS spectra of as-synthesized and air-oxidized 2D SnO_x nanosheets exhibit a characteristic four-peaked structure (labelled as peaks I, II, III, and IV), in which the peaks located at ~2.5 eV (peak I) and ~5 eV (peak II) are associated with Sn 5s and O 2p levels, respectively, whereas peaks at ~7.5 eV (peak III) and ~11 eV (peak IV) are ascribed to Sn 5p – O 2p and Sn 5s – O 2p orbital hybridizations, respectively.[29-31] The presence of peak I is a fingerprint of divalent Sn^{2+} in the as-synthesized 2D nanosheets,[31] and the reduction in the intensity of this peak indicates the post-oxidation of the samples stored in ambient air (Supporting Figure S2b).

Thermal annealing has been demonstrated to significantly impact the morphology, phase composition, and the crystalline structure of metal oxide thin films by reducing lattice disorder lines and vacancies, thereby enhancing their electrical and optical properties.[32-34] We subjected the as-synthesized 2D SnO_x to post-treatment at different temperatures (i.e., 100-450 ºC) and time points (i.e., 15-60 mins). Based on preliminary experiments, we observed from VB-XPS spectra that annealing at 450 ºC for 15 min in an ambient atmosphere can effectively transform SnO into SnO_2 (Supporting Figure S3-5). Henceforth, unless otherwise stated, post-thermal annealing at 450 °C for 15 mins was selected for further experiments.

The chemical composition and crystal phase transformation of 2D SnO_x nanosheets following annealing were evaluated using XPS and Raman spectroscopy. Figure 1c, d displays the XPS analysis of as-synthesized and annealed samples, respectively. The deconvolution of the Sn $3d_{5/2}$ peak reveals two major components centred on 486.1 eV and 486.9 eV for the as-deposited samples (Figure 1c), which can be assigned to Sn^{2+} and Sn^{4+}, respectively, indicating the presence of a mixture of SnO and SnO_2.[35] In contrast, only one component at 486.9 eV, corresponding to Sn^{4+} states, can be seen after the thermal-annealing process. No obvious evidence of a contribution of elemental Sn^0 atoms at ~485 eV was detected in either sample. XPS survey scans and deconvoluted O 1s spectra can be found in Supporting Figure S6-7, in which the O 1s spectra reveals various oxygen species, including O-Sn (530.7 eV), O-Si (532.4 eV), O-C (533.3 eV), and O=C (531.6 eV). Raman spectra of as-deposited 2D SnO_x nanosheets feature two strong Raman peaks at ~211 cm^{-1} and ~618 cm^{-1}, corresponding to A_{1g} modes in SnO and SnO_2, respectively (Figure 1e).[36, 37] As expected, the A_{1g} mode of SnO disappears in the annealed samples, indicating a phase transition from the initial mixture of SnO and SnO_2 to a predominantly SnO_2 structure at the annealing temperature of 450 ^oC. Moreover, the peak at ~618 cm^{-1} not only represents the A_{1g} mode in tetragonal rutile SnO_2 but also indicates the existence of bridging oxygen vacancies in the non-stoichiometric SnO_2 structure.[37]

The optical properties of as-synthesized and annealed 2D nanosheets were explored using UV-Vis spectroscopy. Figure 1f illustrates the shift in the optical band gap of the as-deposited and annealed tin oxide nanosheets. The Tauc plot of the unannealed nanosheets reveals an absorption feature in the range between 3-4 eV, closely associated with the stoichiometry and structural defects of SnO.[20, 38, 39] On the other hand, the annealed sample has a steep absorption edge in the UV region with a direct optical bandgap of ~4.0 eV, consistent with the previous literature.[40] The increase in the optical bandgap from ~3.0 eV to ~4.0 eV following thermal treatment could be attributed to either the rapid reduction in the number of defect states near the band edge due to improved crystallinity or the depletion of Sn^{2+} states.[41] It is worth noting that optical characterization of thermally-annealed nanosheets reveals excellent transparency (>99% transmittance) in the visible to near-infrared range (Supporting Figure S8) thereby, underscoring the potential of LM-printing for the fabrication of transparent electronic devices.

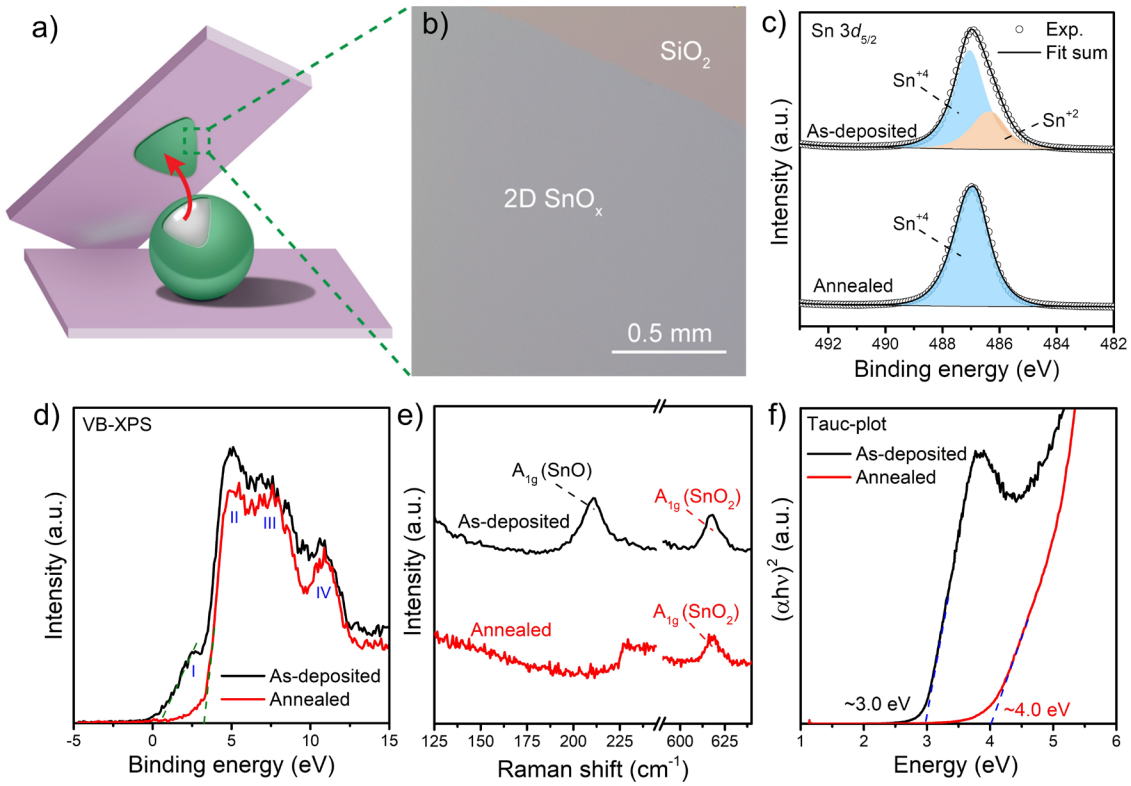

Figure 1. Synthesis and characterizations of 2D tin oxide before and post annealing at 450 ºC for 15 min in air. (a) Schematic illustration of the touch printing technique for the synthesis of ultrathin tin oxide (SnO_x). (b) The optical image of 2D SnO_x prepared on 300 nm SiO_2/Si substrate. (c) XPS spectra in the Sn $3d_{5/2}$ region of the fresh and annealed 2D nanosheets. (d) XPS valence band spectra and (e) Raman spectra of as-synthesized and annealed 2D tin oxide nanosheets printed on 300 nm SiO_2/Si substrate. (f) Tauc plot analysis for the unannealed and annealed 2D SnO_x nanosheets. Annealing was performed at 450 ºC for 15 min in air.

To further elucidate the impact of thermal annealing on improving the structural and optical characteristics of 2D SnO_x nanosheets, atomic force microscopy (AFM) and transmission electron microscopy (TEM) have been conducted to investigate the morphological and crystalline structure of the nanosheets. Three batches of freshly synthesized 2D SnO_x samples were prepared on SiO_2/Si substrates and subjected to thermal annealing at 450 ºC in ambient air for different durations.

AFM images in Figure 2a-c illustrate the evolution of 2D SnO_x nanosheets following the thermal treatment at 450 ºC. As can be seen, all nanosheets exhibit continuous ultrathin features, exceeding

several micrometres. Additionally, minimal wrinkles, folds, pinholes, and cracks can be detected within the scanned areas. Based on the AFM height profiles displayed in the bottom left insets, fresh and annealed samples exhibit a thickness down to ~2.0 nm (with a standard deviation: 0.1 nm) with no significant changes after the annealing process. However, high magnification AFM imaging of as-deposited samples reveals a "fish scale-like" morphology on the 2D SnO_x nanosheets. Interestingly, these small "fish scales" were observed to be gradually dissolved and absorbed into the 2D nanosheets during the high-temperature annealing process (Figure 2a-c, bottom right insets). However, no significant changes in the morphology were observed for annealing durations beyond 15 mins. The average surface roughness of the unannealed and annealed (15 min at 450 ºC) 2D nanosheets was found to be 0.84 nm and 0.72 nm, respectively. These findings are consistent with the TEM analysis detailed in Figure 2d-i and Supporting Figure S9-10. High-Resolution TEM (HRTEM) permits examination of the precise modifications and transformations of the nanostructures within the 2D nanosheets (Figure 2f-g). It is clear that the as-deposited samples shown in Figure 2f and Supporting Figure S9 consist of both amorphous and crystalline heterophases with several grain boundary regions. The selected area electron diffraction (SAED) pattern in the inset of Figure 2f reveals the mixed compositions of tin oxide, supporting the XPS data discussed above. We found that thermal annealing (15 min at 450 ºC) resulted in a polycrystalline structure of 2D SnO_x and significantly reduced the grain boundaries (Figure 2f-g and Supporting Figure S10). The *d*-spacings observed in the annealed nanosheets were found to be of 0.34 and 0.27 nm (Figure 2h-i), corresponding to the (110) and (101) planes in rutile tetragonal SnO_2.[24] More importantly, as the 2D films evolved through thermal annealing, intergranular distorted regions as well as amorphous regions observed in as-made SnO_x samples were significantly reduced (Supporting Figure S10). A small amount of the intermediary Sn_3O_4 phase[42] persists in the samples after annealing, as indicated by the less-pronounced diffraction spots in the inset of Figure 2g. The presence of such Sn_3O_4 phase has been previously reported. [42-44]

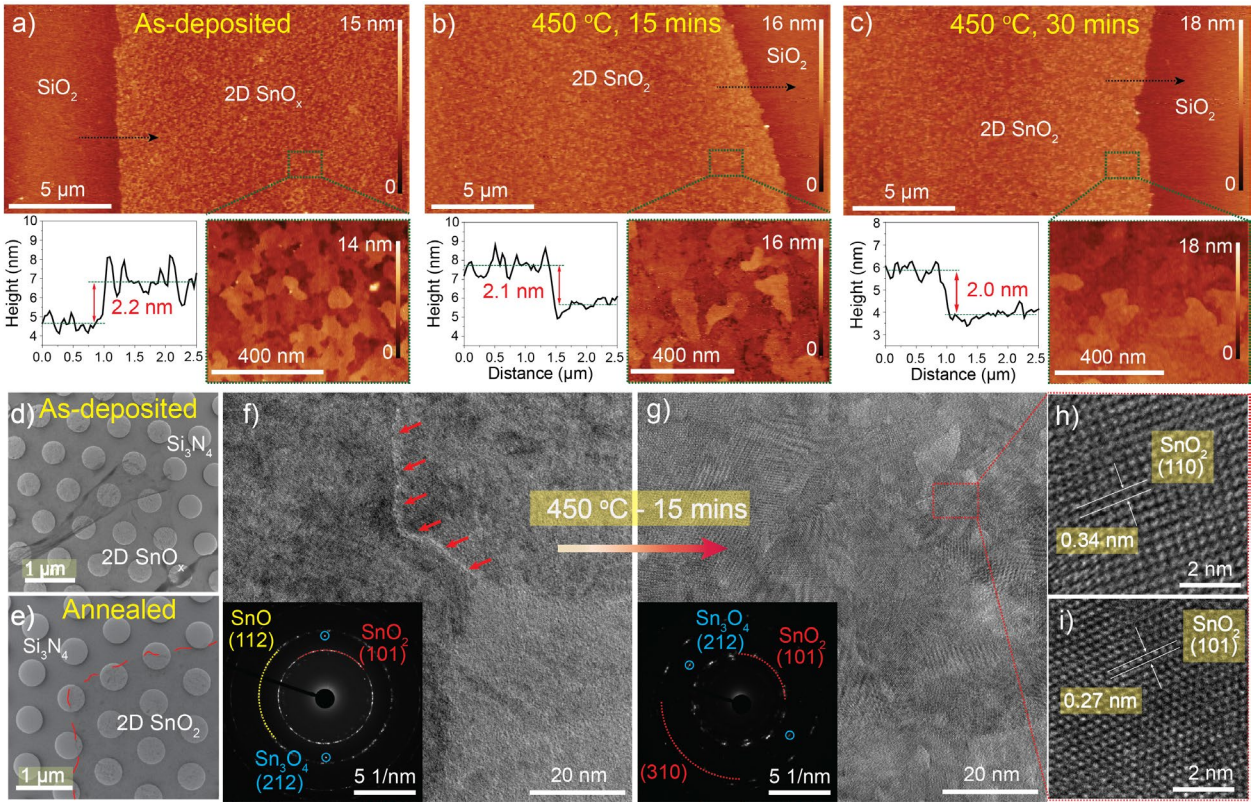

Figure 2. Structural evolution of 2D tin oxides while subjected to the thermal annealing process. (a-c) AFM images of ultrathin SnO_x nanosheets at different anneal conditions with the corresponding step height profiles (lower left insets) and zoomed-in regions (lower right insets). (d-e) Low resolution TEM analysis of as-deposited and annealed nanosheets. (f) HRTEM of as-deposited nanosheet. Red arrows in (f) indicate a distorted boundary region. SAED pattern in (f, inset) signifies the presence of mixed-oxide phases. (g-i) HRTEM analysis of annealed oxide nanosheets. SAED pattern in (g, inset) and HRTEM images in (h, i) indicate the domination of tetragonal SnO_2.

In order to demonstrate the application of 2D tin oxide films to device technology, back-gated field-effect transistors (FETs) were fabricated using 2D SnO_2 (annealed at 450 °C for 15 min) as the semiconducting channel (Figure 3a, inset). Drain characteristics (I_{DS} versus V_{DS}) and transfer characteristics (I_{DS} versus V_{GS}) displayed in Figure 3a-b show the electrical performance of the annealed nanosheets. The FET performance of an unannealed 2D SnO_x-based transistor is shown in Supporting Figure S11, featuring *p*-type FET characteristics with a very low mobility and on-off ratio consistent with the previously reported value.[20] Upon thermal annealing, the transistor performance was remarkably improved (Figure 3a-b). The annealed tin oxide device clearly

showed *n*-type semiconducting behaviour where transfer curves showed a significant increase in the drain current upon increasing the positive gate and drain voltage. The mobilities of the as-deposited and annealed samples were calculated to be ~0.07 $cm^2\ V^{-1}\ s^{-1}$ and ~7.5 $cm^2\ V^{-1}\ s^{-1}$, respectively, revealing a ~100 times mobility enhancement after annealing. The field-effect mobility was calculated using the expression

$$\mu = \frac{L}{W}\frac{dI_{DS}}{dV_{GS}}\frac{1}{V_{DS}C_{ox}} \quad (1)$$

where I_{DS}, V_{DS} *and* V_{GS} are the drain-source current, the drain-source voltage and the gate-source voltage, respectively[45-47]. The channel length (L) and width (W) were 10 μm and 40 μm for all devices, respectively. The capacitance per unit area between the channel and the back gate (C_{ox}) was calculated to be 11.5×10^{-9} F cm^{-2} for the 300 nm thick SiO_2 layer. We find that an annealing duration of 15 min provides a promising on/off ratio of ~10^2. The FET mobility statistics based on different batches of 2D SnO_2 exhibit highly consistent behaviour with a value of 6.98 ± 1.40 $cm^2\ V^{-1}\ s^{-1}$ (Supporting Figure S12). A summary of the field effect electron mobility for previously reported SnO_2 and other metal oxide films is provided in Supporting Table S2. Although the FET performance of the device reported here is not the highest, the annealed 2D SnO_2 significantly surpasses many previously reported transparent semiconducting oxide films. Better device performance can be achieved either by optimizing the semiconductor - insulator interface by using a high-*k* dielectric layer or engineering the device architecture.[48-52]

The enhancement of the device performance is a result of annealing, which significantly influences the growth of crystalline domains and grain boundaries, already supported by the data from TEM and AFM analysis. Additionally, the enhancement in the output drain current is consistent with a substantial reduction in defects in the channel.[53] To provide further information, photoluminescence (PL) studies were carried out to investigate the defect states of the nanosheets using an excitation wavelength of 532 nm under ambient conditions. The excitation energy is found to be lower than the band gap of samples. Hence, defect states are only probed in Supporting Figure S13. A strong PL signal at around 2 eV is observed for the as-prepared tin oxide films, which can be attributed to electronic transitions enabled by the defects levels in the band gap, such as oxygen vacancies, interstitials or dangling bonds in the film.[54, 55] Remarkably, the PL intensity around 2 eV significantly decreased in the annealed samples (450 °C, 15 min), suggesting that

some of the defect centres arising from the presence of mixed SnO and SnO_2 leading to luminescence have been removed, probably by in-diffused oxygen recombining with oxygen vacancies during the annealing process.

Inspired by previous work that has reported the enhancement in the performance of UV photodetectors following annealing,[56, 57] we investigated the photodetection performance of annealed nanosheets (450 °C, 15 min) by irradiating two-terminal planar devices with light emitting diode (LED) sources of 285 nm and 365 nm (Figure 3c-d). In addition to an increased photocurrent (I_{Light}), the process of thermal annealing enhances the photoresponsivity (R), in contrast to their as-deposited counterparts (Supporting Figure S14). The responsivity of post-annealed 2D SnO_2 was determined to be 5.2×10^3 and 6.7×10^2 AW^{-1} when irradiated with wavelengths of 285 nm and 365 nm, respectively. While the responsivity of unannealed nanosheets was determined to be 0.5 AW^{-1} when irradiated with 365 nm wavelength. Figure 3d shows the photocurrent of the device at a wavelength of 285 nm at three different values of the incident light power featuring the dependence of I_{light} on the illumination power intensity.[58]

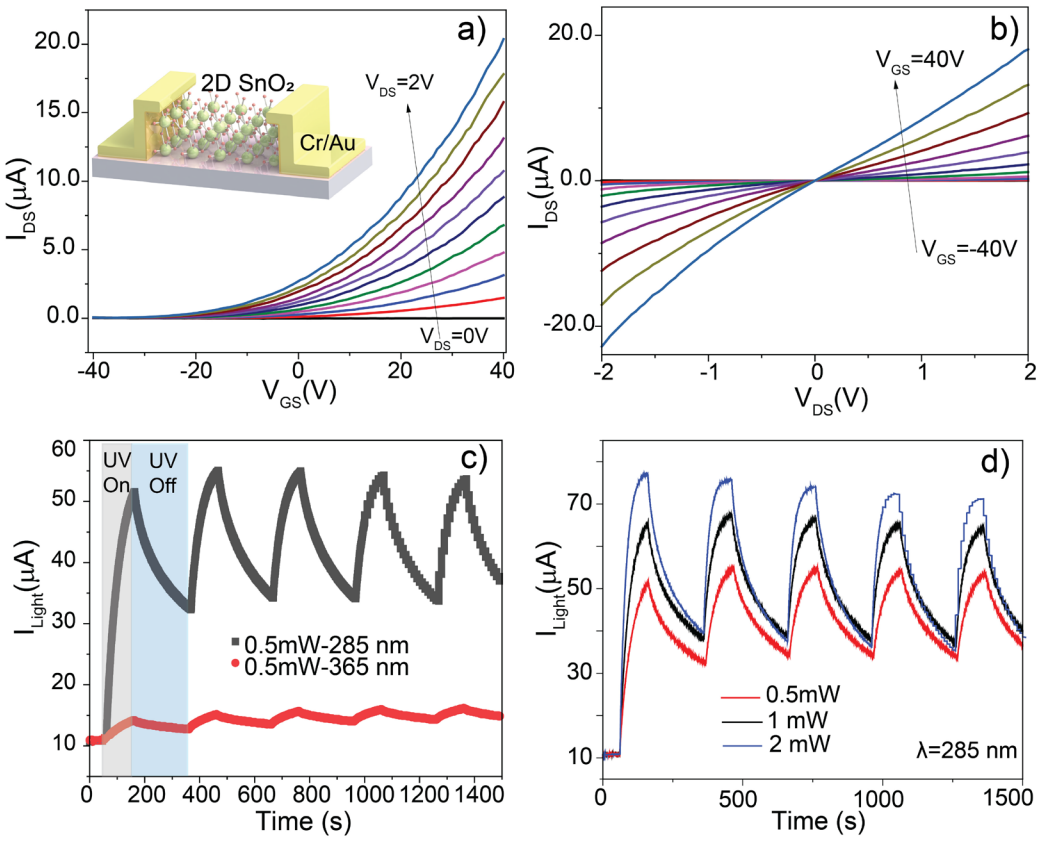

Figure 3. Electronic and optoelectronic performance of the 2D SnO_2 nanosheets annealed at 450 °C for15min. (a-b) FET performance of a device based on annealed tin oxide nanosheet. The inset in (a) shows the schematic structure of the device. (a) Transfer curves with V_{DS} ranging from 0 to 2 V.(b) Output characteristic curves when V_{GS} varies from -40 to 40 V. (c) On/off switching photocurrent cycles of a photodetector based on annealed tin oxide nanosheet measured at 285 nm and 365 nm UV exposure with a power intensity of 0.5 mW cm^{-2} and a bias voltage of 0.5 V. (d) Transient photocurrent as a function of different power intensities measured at a wavelength of 285 nm.

Conclusion

In summary, we report a simple and scalable method for synthesizing large-area and ultrathin 2D tin oxide nanosheets with SnO_2 as the dominant phase. The resulting 2D sheets exhibited a polycrystalline nature with a thickness of ~2 nm covering an area of several square millimetres. Thermal annealing at 450 °C significantly influenced the phase composition and crystalline structure of the tin oxide thin films. FETs were fabricated using 2D SnO_2 as the semiconducting channel, leading to a significant improvement in electron mobility compared to the unannealed nanosheets. The obtained FETs based on 2D SnO_2 showed *n*-type conduction exhibiting a carrier mobility of ~ 7.5 $cm^2 V^{-1} s^{-1}$. UV-detectors based on annealed samples also showed superior photoresponsivity than that of the freshly printed tin oxides. The thermal annealing process showed a significant reduction of intergranular distorted regions and defect states, resulting in a pronounced channel quality improvement leading to enhanced electrical and optical properties. This study provides a roadmap for gaining better control and improved insight into the deposition of ultrathin 2D SnO_2 nanosheets in an ambient environment and is also likely to give access to other tin-based 2D materials. In addition, the developed LM printing technique is highly compatible with existing pattern and etching techniques. This highlights the potential for fabricating large-area device arrays based on ultrathin materials for high-performance and high-density integrated circuits, such as image sensors and artificial synapses. Moreover, this work opens new avenues for emerging transparent electronic and optoelectronic applications.

Experimental Section

Materials

Elemental tin (99.9%) was purchased from Roto Metal. All solvents were obtained from Merck Millipore and used as received. Conducting silicon wafers (300 nm SiO_2/ p^+ Si) were purchased from D&X Co., Ltd. Thermally and mechanically robust silicon nitride (Si_3N_4) TEM grids were obtained from Ted Pella, Inc.

Synthesis of 2D tin oxide nanosheets

A van der Waal touch printing technique was utilized to synthesize ultrathin tin oxide sheets by adapting previously reported studies.[20] Prior to the synthesis, all substrates were sequentially washed with acetone/isopropanol/water and preheated on a hot plate to 280-300 °C. The printing was performed under ambient conditions. Bulk tin metal was placed on a glass slide, and the temperature of the hot plate was set at 280 °C. In order to remove any pre-existing oxide layers with possible airborne contaminants and to expose a pristine metal surface, the liquid tin was preconditioned by squeezing the melt between two glass slides (see Supporting Figure S1a). The freshly formed interfacial oxide layer can be exfoliated from the liquid tin by touching the surface with a suitable substrate (e.g., SiO_2/Si, glass, and quartz substrates). It is worth noting that the exfoliation of 2D SnO_x was performed at 280-300 ^oC as 2D nanosheets produced at higher temperatures (e.g., 450 ^oC) resulted in the fast cumulation of 2D oxide sheets on top of one another, leading to patchy inconsistent morphologies. In addition, XPS data of 2D SnO_x nanosheets produced at 450 ^oC showed the presence of both Sn^{2+} (~6 at%) and Sn^{4+} phases (Supporting Figure. S15). Hence, the synthesis of all 2D tin oxide nanosheets was conducted at 280-300 °C.

For TEM analysis, 2D SnO_x nanosheets were directly transferred onto TEM grids by gently touching the liquid tin. The obtained materials were subjected to annealing on a hotplate at a range of temperatures and durations under ambient condition.

Characterization of 2D tin oxide nanosheets

Optical images: All optical images were obtained using a Leica DM2500 microscope.

XPS: Samples were prepared on SiO_2/Si substrates and examined using an XPS spectrometer (Thermo Scientific) equipped with a monochromatic Al K-alpha source (hv = ~1486.6 eV) and a concentric hemispherical analyzer. Casa-XPS software was utilized to process the obtained data.

AFM: Samples were prepared on SiO_2/Si substrates and subjected to AFM analysis using a Bruker Dimension Icon AFM (ScanAsyst-air mode). The thickness of 2D nanosheets and the surface morphology were acquired using Gwyddion 2.55 software.

TEM: Samples were prepared on Si_3N_4 grids, and TEM analysis was performed on a JEOL JEM-2100F TEM at 200 kV acceleration voltage. Gatan Digital Micrograph software was used to analyze the data.

UV-Vis: Samples were prepared on UV-transparent quartz substrates. All measurements were carried out using a UV-vis spectrophotometer (Agilent Cary 60).

Raman: Samples were prepared on SiO_2/Si substrates. Raman spectra were obtained by employing a Raman spectrometer (Horiba Scientific) with a 532 nm laser source and 1800 mm^{-1} grating.

PL: PL spectra were acquired using a custom-built confocal fluorescence microscope. All optical filters described in the following were acquired from Semrock, USA. A collimated laser beam (532 nm wavelength, gem532, Laser Quantum, UK) was briefly passed through a 532 nm laser line filter (LL01-532,) and focused onto the sample using a 100× air objective. The PL was separated from the excitation signal using a 532 nm dichroic and long-pass filter and detected with a spectrometer (Princeton Instruments, Spectra-Pro with a PIXIS CCD camera) to obtain PL spectra.

Device fabrication and measurement

Back-gated FETs based on ultrathin SnO_x nanosheets were fabricated *via* a photolithography process. Heavily doped (p+) Si wafer was used as the back gate electrode with 300 nm thick SiO_2 as the dielectric layer. Tin dioxide nanosheets were deposited on this 300 nm thick SiO_2/p^+ Si substrates. Next, the obtained nanosheets were subjected to post-annealing at 450 °C for 15 minutes in ambient air before any device fabrication. The samples were first spin-coated with AZ 5214E photoresist prior to electrode patterning utilizing a maskless aligner (Heidelberg-MLA150). After development in an AZ-400K solution (used in a 1:4 dilution), the samples were subjected to Cr/Au (10/100 nm) electrode deposition using an e-beam evaporator (PVD75 - Kurt J. Lesker) and a lift-off process utilising acetone. The FET measurements were conducted using a probe station equipped with a source/measure unit (SMU-Keysight B2902A Precision). Here, the dimensions of

the active channel were assumed to be the length and width of the fabricated electrodes. The carrier mobility could be slightly overestimated due to fringing currents. However, the obtained values are sufficient to examine the effect of thermal annealing on the overall electronic properties of LM-derived 2D SnO_x.

Optoelectronic measurements were performed using commercial monochromatic light-emitting diodes (Thorlabs, Inc.). All device measurements were carried out at ambient conditions. All optical measurements were performed in ambient conditions and LED sources (Thorlabs Inc.) were used to determine the UV photocurrent of the devices at 285 and 365 nm wavelengths. The power intensity was 0.5 $mW.cm^{-2}$ and the bias voltage was 0.5 V. A commercial UV power meter (Newport Corporation) aided in incident power calibration. The photoresponsivity R was extracted from the photodetector performance using the expression:[46]

$$R = \frac{I_{ph}}{PA} \qquad (2)$$

where I_{ph}, P, and A, are the photocurrent relative to the dark current I_{dark}, the incident power density, and the effective illuminated area. Note that specifically $I_{ph} = I_{light} - I_{dark}$ where I_{light} is the measured photocurrent on illumination.

AUTHOR INFORMATION

Corresponding Author

* E-mail: nitu.syed@unimelb.edu.au, chung.nguyen2@rmit.edu.au

Author Contributions

§N.S. and C.K.N. contributed equally.

ASSOCIATED CONTENT

Supporting Information. The Supporting Information is available free of charge at https://pubs.acs.org and contains: synthesis of tin oxide nanosheets; XPS analysis of tin oxide

nanosheets before and after annealing; XPS valence band spectra; Optical characterization of thermal-annealed 2D nanosheets; TEM and HRTEM analysis of unannealed and thermal-annealed 2D nanosheets; FET performance of unannealed and annealed tin oxide; PL spectra of tin oxide nanosheets in visible region; UV photodetection performance of unannealed SnO_x; overview of studies on liquid metal-derived 2D SnO_x nanosheets and their devices.

Acknowledgements

N. S. recognizes the support of a McKenzie Postdoctoral Fellowship from the University of Melbourne. T. D. and C. K. N. acknowledge funding received from the Australian Research Council's (ARC) DECRA program (DE190100100). C. K. N. and A. T. N. acknowledge Ho Chi Minh City University of Technology (HCMUT), VNU-HCM for supporting this study. P.R. acknowledges support through an Australian Research Council DECRA Fellowship (grant no. DE200100279) and an RMIT University Vice-Chancellor's Senior Research Fellowship. A.R. acknowledges support through ARC Centre of Excellence for Transformative Meta-Optical Systems (project number CE200100010). The authors would also like to thank the RMIT Microscopy and Microanalysis Facility (RMMF) and the Micro Nano Research Facility (MNRF).

Conflict of interest

The authors declare no conflict of interest.

References

1. Zavabeti, A.; Jannat, A.; Zhong, L.; Haidry, A. A.; Yao, Z.; Ou, J. Z., Two-Dimensional Materials in Large-Areas: Synthesis, Properties and Applications. *Nano-Micro Lett.* **2020,** *12* (1), 66.
2. Kalantar-zadeh, K.; Ou, J. Z.; Daeneke, T.; Mitchell, A.; Sasaki, T.; Fuhrer, M. S., Two Dimensional and Layered Transition Metal Oxides. *Appl. Mater. Today* **2016,** *5*, 73-89.
3. Xie, H.; Li, Z.; Cheng, L.; Haidry, A. A.; Tao, J.; Xu, Y.; Xu, K.; Ou, J. Z., Recent Advances in the Fabrication of 2D Metal Oxides. *iScience* **2022,** *25* (1), 103598.

4. Yang, T.; Song, T. T.; Callsen, M.; Zhou, J.; Chai, J. W.; Feng, Y. P.; Wang, S. J.; Yang, M., Atomically Thin 2D Transition Metal Oxides: Structural Reconstruction, Interaction with Substrates, and Potential Applications. *Adv. Mater. Interfaces* **2019,** *6* (1), 1801160.
5. Kumbhakar, P.; Chowde Gowda, C.; Mahapatra, P. L.; Mukherjee, M.; Malviya, K. D.; Chaker, M.; Chandra, A.; Lahiri, B.; Ajayan, P. M.; Jariwala, D.; Singh, A.; Tiwary, C. S., Emerging 2D Metal Oxides and their Applications. *Mater. Today* **2021,** *45*, 142-168.
6. Zhou, K.; Shang, G.; Hsu, H. H.; Han, S. T.; Roy, V. A.; Zhou, Y. J. A. M., Emerging 2D Metal Oxides: From Synthesis to Device Integration. *Adv. Mater.* **2023**, 2207774.
7. Timmerman, M. A.; Xia, R.; Le, P. T.; Wang, Y.; Ten Elshof, J. E., Metal Oxide Nanosheets as 2D Building Blocks for the Design of Novel Materials. *Chem. - Eur. J.* **2020,** *26* (42), 9084-9098.
8. Batool, S.; Idrees, M.; Han, S. T.; Roy, V. A.; Zhou, Y., Electrical Contacts With 2D Materials: Current Developments and Future Prospects. *Small* **2023,** *19* (12), 2206550.
9. Carey, B. J.; Ou, J. Z.; Clark, R. M.; Berean, K. J.; Zavabeti, A.; Chesman, A. S. R.; Russo, S. P.; Lau, D. W. M.; Xu, Z.-Q.; Bao, Q.; Kavehei, O.; Gibson, B. C.; Dickey, M. D.; Kaner, R. B.; Daeneke, T.; Kalantar-Zadeh, K., Wafer-Scale Two-Dimensional Semiconductors from Printed Oxide Skin of Liquid Metals. *Nat. Commun.* **2017,** *8* (1), 14482.
10. Cabrera, N.; Mott, N. F., Theory of the Oxidation of Metals. *Rep. Prog. Phys.* **1949,** *12* (1), 163.
11. Goff, A.; Aukarasereenont, P.; Nguyen, C. K.; Grant, R.; Syed, N.; Zavabeti, A.; Elbourne, A.; Daeneke, T., An Exploration into Two-Dimensional Metal Oxides, and other 2D materials, Synthesised *via* Liquid Metal Printing and Transfer Techniques. *Dalton Trans.* **2021,** *50* (22), 7513-7526.
12. Zhao, S.; Zhang, J.; Fu, L., Liquid Metals: A Novel Possibility of Fabricating 2D Metal Oxides. *Adv. Mater.* **2021,** *33* (9), 2005544.
13. Aukarasereenont, P.; Goff, A.; Nguyen, C. K.; McConville, C. F.; Elbourne, A.; Zavabeti, A.; Daeneke, T., Liquid Metals: An Ideal Platform for the Synthesis of Two-Dimensional Materials. *Chem. Soc. Rev.* **2022,** *51* (4), 1253-1276.
14. Karbalaei Akbari, M.; Verpoort, F.; Zhuiykov, S., State-of-the-Art Surface Oxide Semiconductors of Liquid Metals: An Emerging Platform for Development of Multifunctional Two-Dimensional Materials. *J. Mater. Chem. A* **2021,** *9* (1), 34-73.
15. Man Hou, V.; Minsik, K.; Unyong, J.; Michael, D. D. In *Continuous Large Area Oxide Printing from Liquid Metals*, Proc.SPIE, 2023; p 124970R.
16. Du, Y.; Yin, S.; Li, Y.; Chen, J.; Shi, D.; Guo, E.; Zhang, H.; Wang, Z.; Qin, Q.; Zou, C.; Zhai, T.; Li, L., Liquid-Metal-Assisted Synthesis of Patterned GaN Thin Films for High-Performance UV Photodetectors Array. *Small Methods* **2023**, e2300175.
17. Hamlin, A. B.; Ye, Y.; Huddy, J. E.; Rahman, M. S.; Scheideler, W. J., 2D Transistors Rapidly Printed from the Crystalline Oxide Skin of Molten Indium. *npj 2D Mater. Appl.* **2022,** *6* (1), 16.
18. Syed, N.; Zavabeti, A.; Messalea, K. A.; Della Gaspera, E.; Elbourne, A.; Jannat, A.; Mohiuddin, M.; Zhang, B. Y.; Zheng, G.; Wang, L.; Russo, S. P.; Esrafilzadeh, D.; McConville, C. F.; Kalantar-Zadeh, K.; Daeneke, T., Wafer-Sized Ultrathin Gallium and Indium Nitride Nanosheets through the Ammonolysis of Liquid Metal Derived Oxides. *J. Am. Chem. Soc.* **2019,** *141* (1), 104-108.

19. Atkin, P.; Orrell-Trigg, R.; Zavabeti, A.; Mahmood, N.; Field, M. R.; Daeneke, T.; Cole, I. S.; Kalantar-Zadeh, K., Evolution of 2D Tin Oxides on the Surface of Molten Tin. *Chem. Commun.* **2018,** *54* (17), 2102-2105.
20. Daeneke, T.; Atkin, P.; Orrell-Trigg, R.; Zavabeti, A.; Ahmed, T.; Walia, S.; Liu, M.; Tachibana, Y.; Javaid, M.; Greentree, A. D.; Russo, S. P.; Kaner, R. B.; Kalantar-Zadeh, K., Wafer-Scale Synthesis of Semiconducting SnO Monolayers from Interfacial Oxide Layers of Metallic Liquid Tin. *ACS Nano* **2017,** *11* (11), 10974-10983.
21. Nguyen, C. K.; Taylor, P. D.; Zavabeti, A.; Alluhaybi, H.; Almalki, S.; Guo, X.; Irfan, M.; Kobaisi, M. A.; Ippolito, S. J.; Spencer, M. J. S.; Balendhran, S.; Roberts, A.; Daeneke, T.; Crozier, K. B.; Sabri, Y.; Syed, N., Instant-in-Air Liquid Metal Printed Ultrathin Tin Oxide for High-Performance Ammonia Sensors. *Adv. Funct. Mater.*, 2309342.
22. Datta, R. S.; Syed, N.; Zavabeti, A.; Jannat, A.; Mohiuddin, M.; Rokunuzzaman, M.; Yue Zhang, B.; Rahman, M. A.; Atkin, P.; Messalea, K. A.; Ghasemian, M. B.; Gaspera, E. D.; Bhattacharyya, S.; Fuhrer, M. S.; Russo, S. P.; McConville, C. F.; Esrafilzadeh, D.; Kalantar-Zadeh, K.; Daeneke, T., Flexible Two-Dimensional Indium Tin Oxide Fabricated Using a Liquid Metal Printing Technique. *Nat. Electron.* **2020,** *3* (1), 51-58.
23. Yuan, T.; Hu, Z.; Zhao, Y.; Fang, J.; Lv, J.; Zhang, Q.; Zhuang, Z.; Gu, L.; Hu, S., Two-Dimensional Amorphous SnO_x from Liquid Metal: Mass Production, Phase Transfer, and Electrocatalytic CO_2 Reduction toward Formic Acid. *Nano Lett.* **2020,** *20* (4), 2916-2922.
24. Huang, C.-H.; Chang, H.; Yang, T.-Y.; Wang, Y.-C.; Chueh, Y.-L.; Nomura, K., Artificial Synapse Based on a 2D-SnO_2 Memtransistor with Dynamically Tunable Analog Switching for Neuromorphic Computing. *ACS Appl. Mater. Interfaces* **2021,** *13* (44), 52822-52832.
25. Lee, D. J.; Lee, S.; Kim, D. Y., Sturdy Memristive Switching Characteristics of Flexible 2D SnO Prepared by Liquid-to-Solid Exfoliation. *Ceram. Int.* **2021,** *47* (20), 28437-28443.
26. Li, Q.; Lin, J.; Liu, T.-Y.; Zhu, X.-Y.; Yao, W.-H.; Liu, J., Gas-Mediated Liquid Metal Printing toward Large-Scale 2D Semiconductors and Ultraviolet Photodetector. *npj 2D Mater. Appl.* **2021,** *5* (1), 36.
27. Cheng, Y. F.; Li, Z.; Zhang, M.; Xie, H. G.; Tang, T.; Liang, Y.; Wang, X. X.; Xu, K.; Zhang, B. Y.; Haidry, A. A.; Ou, J. Z., Liquid-Tin-Printed Two-Dimensional SnO for Optoelectronic NO_2 Gas Sensing at Room Temperature. *J. Mater. Chem. C* **2023,** *11* (41), 14187-14198.
28. Allen, J. P.; Scanlon, D. O.; Parker, S. C.; Watson, G. W., Tin Monoxide: Structural Prediction from First Principles Calculations with Van der Waals Corrections. *J. Phys. Chem. C* **2011,** *115* (40), 19916-19924.
29. Themlin, J. M.; ChtaÏB, M.; Henrard, L.; Lambin, P.; Darville, J.; Gilles, J. M., Characterization of Tin Oxides by X-Ray-Photoemission Spectroscopy. *Phys. Rev. B* **1992,** *46* (4), 2460-2466.
30. Nikiforov, A.; Timofeev, V.; Mashanov, V.; Azarov, I.; Loshkarev, I.; Volodin, V.; Gulyaev, D.; Chetyrin, I.; Korolkov, I., Formation of SnO and SnO_2 Phases During the Annealing of SnO(x) Films Obtained by Molecular Beam Epitaxy. *Appl. Surf. Sci.* **2020,** *512*, 145735.
31. Nose, K.; Suzuki, A.; Oda, N.; Kamiko, M.; Mitsuda, Y., Oxidation of SnO to SnO_2 Thin Films in Boiling Water at Atmospheric Pressure. *Appl. Phys. Lett.* **2014,** *104* (9), 091905
32. Zhou, J. X.; Zhang, M. S.; Hong, J. M.; Fang, J. L.; Yin, Z., Structural and Spectral Properties of SnO_2 Nanocrystal Prepared by Microemulsion Technique. *Appl. Phys. A* **2005,** *81* (1), 177-182.

33. Kar, A.; Yang, J.; Dutta, M.; Stroscio, M. A.; Kumari, J.; Meyyappan, M., Rapid Thermal Annealing Effects on Tin Oxide Nanowires Prepared by Vapor–Liquid–Solid Technique. *Nanotechnol.* **2009,** *20* (6), 065704-065704.
34. Nguyen, C. K.; Mazumder, A.; Mayes, E. L.; Krishnamurthi, V.; Zavabeti, A.; Murdoch, B. J.; Guo, X.; Aukarasereenont, P.; Dubey, A.; Jannat, A.; Wei, X.; Truong, V. K.; Bao, L.; Roberts, A.; McConville, C. F.; Walia, S.; Syed, N.; Daeneke, T., 2-nm-Thick Indium Oxide Featuring High Mobility. *Adv. Mater. Interfaces* **2023,** *10* (9), 2202036.
35. Wang, J.; Li, H.; Meng, S.; Ye, X.; Fu, X.; Chen, S., Controlled Synthesis of Sn-based Oxides *via* a Hydrothermal Method and their Visible Light Photocatalytic Performances. *RSC Adv.* **2017,** *7* (43), 27024-27032.
36. Geurts, J.; Rau, S.; Richter, W.; Schmitte, F. J., SnO Films and their Oxidation to SnO_2: Raman Scattering, IR Reflectivity and X-Ray Diffraction Studies. *Thin Solid Films* **1984,** *121* (3), 217-225.
37. Liu, L. Z.; Li, T. H.; Wu, X. L.; Shen, J. C.; Chu, P. K., Identification of Oxygen Vacancy Types from Raman Spectra of SnO_2 Nanocrystals. *J. Raman Spectrosc.* **2012,** *43* (10), 1423-1426.
38. Sethi, R.; Ahmad, S.; Aziz, A.; Siddiqui, A. M., Structural, Optical and Electrical Properties of Tin Oxide Thin Films for Application as a Wide Band Gap Semiconductor. *AIP Conf. Proc.* **2015,** *1675* (1), 030039.
39. Hadia, N. M. A.; Ryabtsev, S. V.; Seredin, P. V.; Domashevskaya, E. P., Effect of the Temperatures on Structural and Optical Properties of Tin Oxide (SnO_x) Powder. *Physica B Condens. Matter.* **2010,** *405* (1), 313-317.
40. Zhang, M.; Xu, M.; Li, M.; Zhang, Q.; Lu, Y.; Chen, J.; Li, M.; Dai, J.; Chen, C.; He, Y., SnO_2 Epitaxial Films with Varying Thickness on C-Sapphire: Structure Evolution and Optical Band Gap Modulation. *Appl. Surf. Sci.* **2017,** *423*, 611-618.
41. Sadeghzadeh-Attar, A.; Bafandeh, M. R., The Effect of Annealing Temperature on the Structure and Optical Properties of Well-aligned 1D SnO_2 Nanowires Synthesized using Template-Assisted Deposition. *Cryst. Eng. Comm* **2018,** *2* (4), 460-469.
42. Liu, Y.-S.; Yamaguchi, A.; Yang, Y.; Aisnada, A. N. E.; Uchida, S.; Abe, H.; Ueda, S.; Yamaguchi, K.; Tanabe, T.; Miyauchi, M., Synthesis and Characterization of the Orthorhombic Sn_3O_4 Polymorph. *Angew. Chem. Int. Ed.* **2023,** *62* (17), e202300640.
43. Huang, P.-H.; Zhang, Z.-X.; Hsu, C.-H.; Wu, W.-Y.; Ou, S.-L.; Huang, C.-J.; Wuu, D.-S.; Lien, S.-Y.; Zhu, W.-Z., Deposition mechanism and characterization of plasma-enhanced atomic layer-deposited SnO x films at different substrate temperatures. *Nanomater.* **2022,** *12* (16), 2859.
44. Hsu, C.-H.; Zhang, Z.-X.; Huang, P.-H.; Wu, W.-Y.; Ou, S.-L.; Lien, S.-Y.; Huang, C.-J.; Lee, M.-K.; Zhu, W.-Z., Effect of Plasma Power on the Structural Properties of Tin Oxide Prepared by Plasma-Enhanced Atomic Layer Deposition. *Ceram. Int.* **2021,** *47* (6), 8634-8641.
45. Jannat, A.; Syed, N.; Xu, K.; Rahman, M. A.; Talukder, M. M. M.; Messalea, K. A.; Mohiuddin, M.; Datta, R. S.; Khan, M. W.; Alkathiri, T.; Murdoch, B. J.; Reza, S. Z.; Li, J.; Daeneke, T.; Zavabeti, A.; Ou, J. Z., Printable Single-Unit-Cell-Thick Transparent Zinc-Doped Indium Oxides with Efficient Electron Transport Properties. *ACS Nano* **2021,** *15* (3), 4045-4053.
46. Nguyen, C. K.; Low, M. X.; Zavabeti, A.; Murdoch, B. J.; Guo, X.; Aukarasereenont, P.; Mazumder, A.; Dubey, A.; Jannat, A.; Rahman, M. A.; Chiang, K.; Truong, V. K.; Bao, L.; McConville, C. F.; Walia, S.; Daeneke, T.; Syed, N., Atomically Thin Antimony-Doped Indium Oxide Nanosheets for Optoelectronics. *Adv. Opt. Mater.* **2022,** *10* (20), 2200925.

47. Tang, Y.; Huang, C.-H.; Nomura, K., Vacuum-Free Liquid-Metal-Printed 2D Indium–Tin Oxide Thin-Film Transistor for Oxide Inverters. *ACS Nano* **2022,** *16* (2), 3280-3289.
48. Wang, B.; Huang, W.; Chi, L.; Al-Hashimi, M.; Marks, T. J.; Facchetti, A., High-k Gate Dielectrics for Emerging Flexible and Stretchable Electronics. *Chem. Rev.* **2018,** *118* (11), 5690-5754.
49. Nomura, K.; Ohta, H.; Ueda, K.; Kamiya, T.; Hirano, M.; Hosono, H., Thin-Film Transistor Fabricated in Single-Crystalline Transparent Oxide Semiconductor. *Science* **2003,** *300* (5623), 1269-1272.
50. Shin, D. H.; Kim, Y.-j.; Lee, S.-K.; Bae, S.; Ahn, S., Atomically Thin Alkane Passivation Layer for Flexible and Transparent Graphene Electronics. *Appl. Surf. Sci.* **2023,** *612*, 155695.
51. Yi, J.; Sun, X.; Zhu, C.; Li, S.; Liu, Y.; Zhu, X.; You, W.; Liang, D.; Shuai, Q.; Wu, Y.; Li, D.; Pan, A., Double-Gate MoS_2 Field-Effect Transistors with Full-Range Tunable Threshold Voltage for Multifunctional Logic Circuits. *Adv. Mater.* **2021,** *33* (27), 2101036.
52. Pang, Y.; Zhou, Y.; Tong, L.; Xu, J., 2D Dual Gate Field-Effect Transistor Enabled Versatile Functions. *Small* **2024,** *20* (2), 2304173.
53. Islam, Z.; Kozhakhmetov, A.; Robinson, J.; Haque, A., Enhancement of WSe_2 FET Performance Using Low-Temperature Annealing. *J. Electron. Mater.* **2020,** *49* (6), 3770-3779.
54. Bonu, V.; Das, A.; Prasad, A. K.; Krishna, N. G.; Dhara, S.; Tyagi, A. J. A. P. L., Influence of In-Plane and Bridging Oxygen Vacancies of SnO_2 Nanostructures on CH_4 Sensing at Low Operating Temperatures. *J. Appl. Phys. Lett.* **2014,** *105* (24), 243102.
55. Nehru, L.; Swaminathan, V.; Sanjeeviraja, C., Photoluminescence Studies on Nanocrystalline Tin Oxide Powder for Optoelectronic Devices. *Am. J. Mater. Sci.* **2012,** *2* (2), 6-10.
56. Wang, J.; Ye, L.; Wang, X.; Zhang, H.; Li, L.; Kong, C.; Li, W., High Transmittance β-Ga_2O_3 Thin Films Deposited by Magnetron Sputtering and Post-Annealing for Solar-Blind Ultraviolet Photodetector. *J. Alloys Compd.* **2019,** *803*, 9-15.
57. Zhou, C.; Liu, K.; Chen, X.; Feng, J.; Yang, J.; Zhang, Z.; Liu, L.; Xia, Y.; Shen, D., Performance Improvement of Amorphous Ga_2O_3 Ultraviolet Photodetector by Annealing under Oxygen Atmosphere. *J. Alloys Compd.* **2020,** *840*, 155585.
58. Qiu, Q.; Huang, Z., Photodetectors of 2D Materials from Ultraviolet to Terahertz Waves. *Adv. Mater.* **2021,** *33* (15), 2008126.

For Table of Contents Use Only